

RESEARCH ARTICLE

# Dissecting the Molecular Mechanism of Nucleotide-Dependent Activation of the KtrAB K<sup>+</sup> Transporter

Andras Szollosi<sup>1#a</sup>, Ricardo S. Vieira-Pires<sup>1#b</sup>, Celso M. Teixeira-Duarte<sup>1,2</sup>, Rita Rocha<sup>1,2</sup>, João H. Morais-Cabral<sup>1,2\*</sup>

**1** IBMC, Instituto de Biologia Molecular e Celular, Universidade do Porto, Porto, Portugal, **2** Instituto de Investigação e Inovação em Saúde, Universidade do Porto, Porto, Portugal

<sup>#a</sup> Current address: Department of Medical Biochemistry, Semmelweis University, Budapest H-1094, Hungary

<sup>#b</sup> Current address: Center for Neuroscience and Cell Biology (CNBC/UC), University of Coimbra, Portugal

\* [jcabral@ibmc.up.pt](mailto:jcabral@ibmc.up.pt)



**OPEN ACCESS**

**Citation:** Szollosi A, Vieira-Pires RS, Teixeira-Duarte CM, Rocha R, Morais-Cabral JH (2016) Dissecting the Molecular Mechanism of Nucleotide-Dependent Activation of the KtrAB K<sup>+</sup> Transporter. *PLoS Biol* 14 (1): e1002356. doi:10.1371/journal.pbio.1002356

**Academic Editor:** Raimund Dutzler, University of Zurich, SWITZERLAND

**Received:** June 4, 2015

**Accepted:** December 10, 2015

**Published:** January 15, 2016

**Copyright:** © 2016 Szollosi et al. This is an open access article distributed under the terms of the [Creative Commons Attribution License](https://creativecommons.org/licenses/by/4.0/), which permits unrestricted use, distribution, and reproduction in any medium, provided the original author and source are credited.

**Data Availability Statement:** Coordinate and diffraction data files are available from the PDB database (accession number 5BUT). Numerical data for Figures 1a-b; 3a-b, 4b-e, 5c-d; S10a-c, and S11a-d are provided in Supplemental Material ([S1 Data](#))

**Funding:** AS was supported by FEBS (Long term fellowship). This work was financially supported by national funds through FCT—Fundação para a Ciência e a Tecnologia/MEC—Ministério da Educação e Ciência and when applicable co-funded by FEDER funds within the Partnership Agreement PT2020 related with the research unit number 4293 and by FEDER funds through the Operational

## Abstract

KtrAB belongs to the Trk/Ktr/HKT superfamily of monovalent cation (K<sup>+</sup> and Na<sup>+</sup>) transport proteins that closely resemble K<sup>+</sup> channels. These proteins underlie a plethora of cellular functions that are crucial for environmental adaptation in plants, fungi, archaea, and bacteria. The activation mechanism of the Trk/Ktr/HKT proteins remains unknown. It has been shown that ATP stimulates the activity of KtrAB while ADP does not. Here, we present X-ray structural information on the KtrAB complex with bound ADP. A comparison with the KtrAB-ATP structure reveals conformational changes in the ring and in the membrane protein. In combination with a biochemical and functional analysis, we uncover how ligand-dependent changes in the KtrA ring are propagated to the KtrB membrane protein and conclude that, despite their structural similarity, the activation mechanism of KtrAB is markedly different from the activation mechanism of K<sup>+</sup> channels.

## Author Summary

Animals have organs that regulate the balance of water and ions in the fluids bathing their cells. In contrast, the cells of plants, bacteria, and fungi have little or no control over those fluids and, thus, they have to cope with changes in the local environment. These cells have therefore evolved specific molecular systems that are crucial for environmental adaptation. We study the molecular properties of the membrane protein KtrAB—a member of the Trk/Ktr/HKT superfamily of transport proteins that shuffle K<sup>+</sup> and Na<sup>+</sup> ions across the plasma membrane, closely resemble K<sup>+</sup> channels, and underlie environmental adaptation of cells of plants, fungi, bacteria, and archaea. KtrAB is formed by the KtrB membrane protein and the KtrA cytosolic ring protein. KtrA binds to both ADP and ATP, resulting in a low-activity ADP-bound state and a high-activity ATP-bound state, respectively. We determined a low resolution structure of a low-activity form of the transport protein. A

Competitiveness Program—COMPETE and by National Funds through FCT—Fundação para a Ciência e a Tecnologia under the project FCOMP-01-0124-FEDER-028115 (PTDC/BBB-BEP/2017/2012). The funders had no role in study design, data collection and analysis, decision to publish, or preparation of the manuscript.

**Competing Interests:** The authors have declared that no competing interests exist.

**Abbreviations:** ADP, adenosine diphosphate; cpm., counts per minute; DEN, Deformable Elastic Network; DTNB, 5,5'-dithio-bis(2-nitrobenzoic acid); KtrA<sub>ΔC</sub>, KtrA protein with C-terminal domain truncated; LLG, log-of-likelihood; M1D2, M1 transmembrane helix in repeat D2; RCK, regulate conductance of K<sup>+</sup>; SEM, standard error of the mean; TNB, thio-nitrobenzoate.

comparison of this structure with the structure of ATP-bound KtrAB reveals changes in both the KtrA ring and the KtrB membrane protein. We uncover how changes in the KtrA ring are propagated to KtrB and conclude that, despite their structural similarity, the activation mechanism of KtrAB is markedly different from the activation mechanism of K<sup>+</sup> channels.

## Introduction

KtrAB belongs to the Trk/Ktr/HKT superfamily of monovalent cation (K<sup>+</sup> and Na<sup>+</sup>) transport proteins that are found ubiquitously in nonanimal cells [1–3]. The Trk/Ktr/HKT superfamily comprises uniporters (K<sup>+</sup> or Na<sup>+</sup>) and symporters (K<sup>+</sup>/Na<sup>+</sup> or K<sup>+</sup>/H<sup>+</sup>) and underlies a plethora of cellular functions in plants, fungi, archaea, and bacteria such as K<sup>+</sup> and Na<sup>+</sup> uptake, regulation of cellular electrical activity, turgor compensation, osmotic adjustment (thereby contributing to resistance to drought and salinity), intra- and intercellular ion transport, motor cellular functions, and adjustment of membrane potential [2,4].

The structure of the KtrAB complex from the bacterium *Bacillus subtilis* was recently determined [5]. This protein complex plays an important role in the osmotic adaptation mechanism of this bacterium [6]. It is composed by a homodimeric KtrB membrane protein (GenBank: KIX81591.1) assembled with the KtrA octameric ring (GenBank: KIX81590.1). KtrB is responsible for ion permeation; each KtrB subunit has the architecture of a potassium channel pore domain [1,5,7] (S1A–S1D Fig), consisting of four M1-P-M2 (transmembrane helix 1-pore helix and loop-transmembrane helix 2) structural repeats (D1 to D4), which embrace an ion-permeable pore. KtrA binds ATP and adenosine diphosphate (ADP) and is responsible for regulation of KtrAB activity [5,8]. This cytosolic protein is a regulate conductance of K<sup>+</sup> (RCK) domain [5,9–11] that assembles as an octameric ring, closely resembling the RCK gating rings of the MthK [12,13], BK [14–16], and GsuK [17] potassium channels (S1E–S1F Fig). The architecture of the KtrAB complex is also present in the TrkHA complex, another member of the Trk/Ktr/HKT superfamily [18].

Importantly, KtrB displays structural features that are not present in K<sup>+</sup> channels. In particular, repeat D3 of KtrB has an insertion of ~10 residues that form an intramembrane loop pointing into the cytosolic pore. This intramembrane loop is also found in other members of the Trk/Ktr/HKT superfamily [1,7,19], and together with a highly conserved arginine residue (R417 in KtrB from *B. subtilis*), it obstructs the ion pathway of KtrAB and TrkHA [5,18,20]. The intramembrane loop and the conserved arginine are thought to be a central feature of the activation mechanism of KtrAB and TrkHA. In KtrB from *Vibrio alginolyticus*, cell-based studies showed that truncations introduced in the intramembrane loop enhance the maximum uptake velocity for K<sup>+</sup> [21]; and an electron paramagnetic resonance study showed a K<sup>+</sup>-dependent relative motion of the intramembrane loop [22]. In TrkH, mutation of the conserved arginine to alanine enhanced K<sup>+</sup> flux in a liposome-based assay [20] and electrophysiological recordings with the TrkHA complex showed that truncation of the intramembrane loop changes the response to the ligand and increases the open probability in the absence of ligand [18]. These results, together with the structures of KtrAB and TrkHA, have led to the proposal that the intramembrane loop and the conserved arginine function as a pore gate.

It has been shown that some orthologs of KtrAB are regulated by cyclic-diAMP [23–25], and additionally, in *B. subtilis*, the KtrAB operon responds to cyclic-diAMP [26]. Importantly, it is generally accepted that activation of KtrAB and TrkHA involves ATP binding to the KtrA and TrkA gating rings, respectively. Structures of isolated KtrA and TrkA rings show ligand-dependent conformational changes. In TrkHA, the open probability increases with ATP and

decreases with ADP [18]. In KtrAB, ion flux is stimulated by ATP and not by ADP; the ADP-bound KtrAB is in a low-activity state, displaying basal activity that is also present in KtrB alone [5,8]. Not much more is understood about the molecular mechanism of activation of these transporters; in particular, the conformational changes induced by ATP and ADP in the KtrAB or TrkHA complexes have not been described.

We present a structure of KtrAB in the low-activity, ADP-bound state and reveal conformational changes in the gating ring and the membrane protein relative to the high-activity ATP-bound KtrAB. We also perform a functional and biochemical characterization of the mechanism of activation. Based on these results, we propose an activation mechanism of the KtrAB complex by ATP.

## Results

### The Structure of the KtrA<sub>ΔC</sub>B Complex

To gain structural insights into the mechanism of activation of the KtrAB K<sup>+</sup> transporter, we crystallized the ADP-bound KtrAB complex from *B. subtilis* but could only measure diffraction data to ~8 Å from these crystals. As an alternative, we turned to the KtrA<sub>ΔC</sub>B complex, which is formed by wild-type KtrB and a C-terminal domain truncated form of KtrA (KtrA<sub>ΔC</sub>). This KtrA form lacks residues 145 to 222 that correspond to the whole C-terminal domain (S1E Fig). Ligand-binding studies show that KtrA<sub>ΔC</sub> from *B. subtilis* is able to bind ATP and ADP and crystal structures have shown that it forms an octameric ring [11]. Also, it has been reported that versions of KtrA<sub>ΔC</sub>B from *V. alginolyticus* are inactive [8]. We verified by size-exclusion chromatography that the complex between KtrB and KtrA<sub>ΔC</sub> is formed both in the presence of ADP and ATP (S2A Fig). We also measured KtrA<sub>ΔC</sub>B-mediated <sup>86</sup>Rb<sup>+</sup> flux using a liposome-based assay (Fig 1A) and compared it with an equivalent characterization of wild type KtrAB (Fig 1B). As demonstrated before [5], ATP stimulates wild type KtrAB flux relative to ADP and to KtrB alone. Despite a larger background signal (a detailed explanation for this observation can be found in Material and Methods), it is clear that after 1 h, KtrA<sub>ΔC</sub>B-mediated <sup>86</sup>Rb<sup>+</sup> uptake levels are identical for KtrA<sub>ΔC</sub>B-ATP and KtrA<sub>ΔC</sub>B-ADP and similar to uptake levels of KtrB alone. Thus, the stimulatory effect of ATP is abolished in KtrA<sub>ΔC</sub>B, leading us to conclude that this complex is trapped in a low-activity state.

We crystallized KtrA<sub>ΔC</sub>B bound to ADP, collected diffraction data to 6 Å (S2 Table), and solved the structure (Protein Data Bank accession number 5BUT) by molecular replacement using the KtrB dimer structure from KtrAB and one of the octameric ring structures previously determined for KtrA<sub>ΔC</sub> [11]. As in the KtrAB-ATP and TrkHA structures, the asymmetric unit contains two membrane-protein dimers associated with opposing faces of an octameric RCK ring [5,18] (S4 Fig). The calculated electron-density map was then 4-fold and 8-fold averaged in the molecular envelopes corresponding to KtrB and KtrA, respectively. The resulting 6 Å electron-density map is of very high quality (Fig 1C), clearly showing the position of all trans-membrane and pore helices in KtrB as well as the position of different secondary-structure elements in the KtrA subunits. The final KtrA<sub>ΔC</sub>B-ADP model (Fig 1D and S4 Fig) was generated by manual adjustment of the M1 helix in the KtrB D2 repeat to better fit the map (more details below) and Deformable Elastic Network (DEN) refinement (S2 Table). The final model fits very well in the averaged electron-density map (Fig 1C).

Importantly, we could establish that KtrA<sub>ΔC</sub>B-ADP and KtrAB-ADP are structurally similar and distinct from KtrAB-ATP. Using as search models a collection of different KtrA<sub>ΔC</sub> ring structures (S5 Fig) and two KtrB structures (from KtrAB-ATP and KtrA<sub>ΔC</sub>B-ADP; Fig 1D and 1E), we performed molecular replacement searches against an 8 Å diffraction dataset collected from wild-type KtrAB-ADP crystals. The six different RCK ring structures together with the

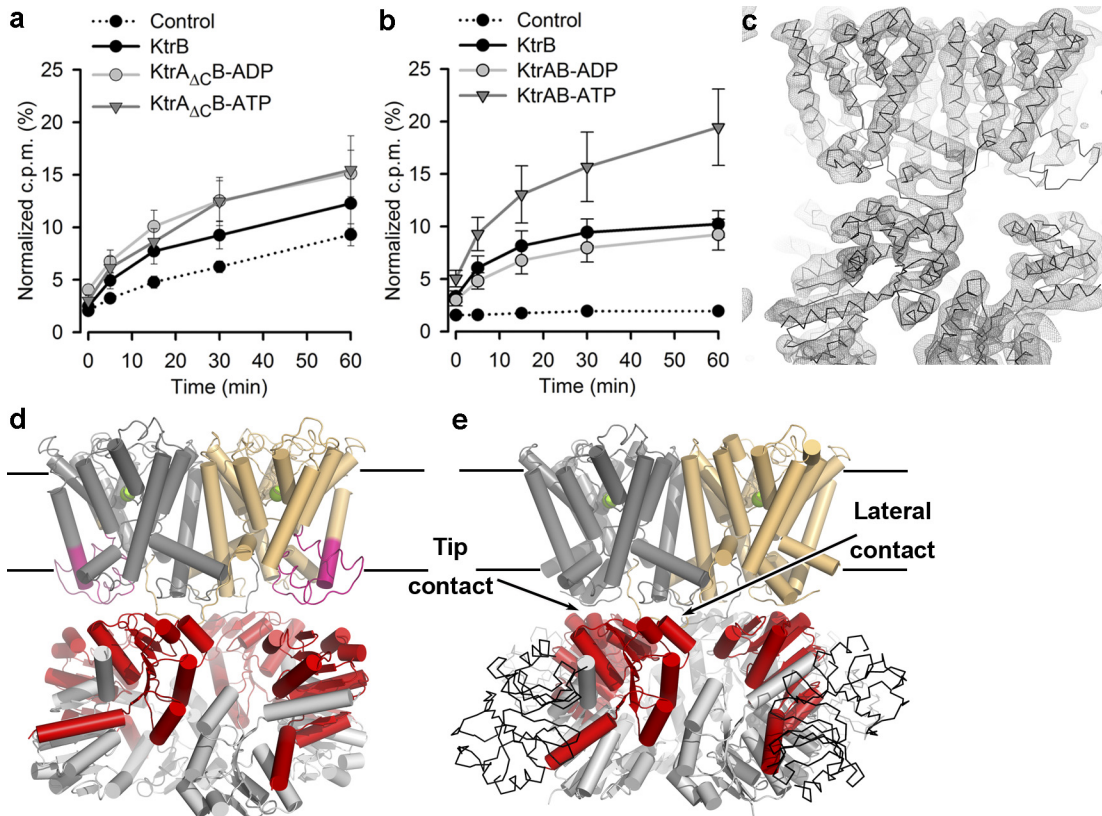


**Fig 1. Structure of KtrA $\Delta$ C B.**  $^{86}\text{Rb}^+$  uptake into proteoliposomes with **a**) KtrA $\Delta$ C B (with ATP or ADP) and KtrB alone (with ATP), or with **b**) wild type KtrAB (with ATP or ADP) and KtrB alone (with ATP). Control liposomes were formed in the presence of KtrA $\Delta$ C or KtrA alone; liposome float-up experiments are shown in [S3 Fig](#); KtrA $\Delta$ C increases liposome leakiness as reflected in the increased control signal (see raw data in [S1 Table](#)). Mean  $\pm$  standard error of the mean (SEM) values calculated from 5–8 assays from 3 separate liposome preparations. counts per minute (cpm). **c**) Averaged electron-density map of KtrA $\Delta$ C B in mesh with superposed Ca trace of refined KtrA $\Delta$ C B structure. Side views of **d**) KtrA $\Delta$ C B-ADP and **e**) wild type KtrAB-ATP. KtrB dimer is shown at the top and colored dark-grey and wheat, with D1-D2 domain of KtrA $\Delta$ C B in magenta. RCK rings are shown in light grey and red with N-terminal domain as cartoon and C-terminal domain in KtrAB-ATP as thin Ca trace; K $^+$  ions as green spheres; tip and lateral contacts are labeled; putative membrane limits are indicated by horizontal lines. Numerical values of data displayed in panels a and b are included in [S1 Data](#).

doi:10.1371/journal.pbio.1002356.g001

two different KtrB structures cover a range of potential conformations of the KtrAB complex and allowed us to get a low resolution model of the KtrAB-ADP structure. The procedure involved sequential searches with the membrane proteins and with the gating rings; for many of these pairs, we were able to obtain molecular replacement solutions that display the expected packing between the membrane protein dimer and the gating ring. The values for the log-of-likelihood (LLG) function (a measure of how well the structural model agrees with the data) are shown in [S3 Table](#); they clearly show that the pair formed by the KtrB homodimer from the KtrA $\Delta$ C B-ADP together with the KtrA $\Delta$ C ring also from the KtrA $\Delta$ C B-ADP (model 7) has the highest LLG value (LLG = 515). A detailed analysis of the significance and sensitivity of LLG values is presented with [S3 Table](#).

Overall, these LLG results ([S3 Table](#)) show that the best fit for the KtrAB-ADP diffraction data is obtained with the protein components of the KtrA $\Delta$ C B-ADP structure, strongly indicating that KtrA $\Delta$ C B-ADP is structurally similar to KtrAB-ADP. In contrast, the pair formed by the KtrB homodimer from KtrAB-ATP and KtrA-ATP (without the C-terminal domain) has a LLG = 223 and incorrect packing, indicating that the ATP-bound complex is structurally distinct from KtrAB-ADP. We also determined an averaged density map for the KtrAB-ADP structure using the starting phases calculated from the KtrA $\Delta$ C B model after rigid body

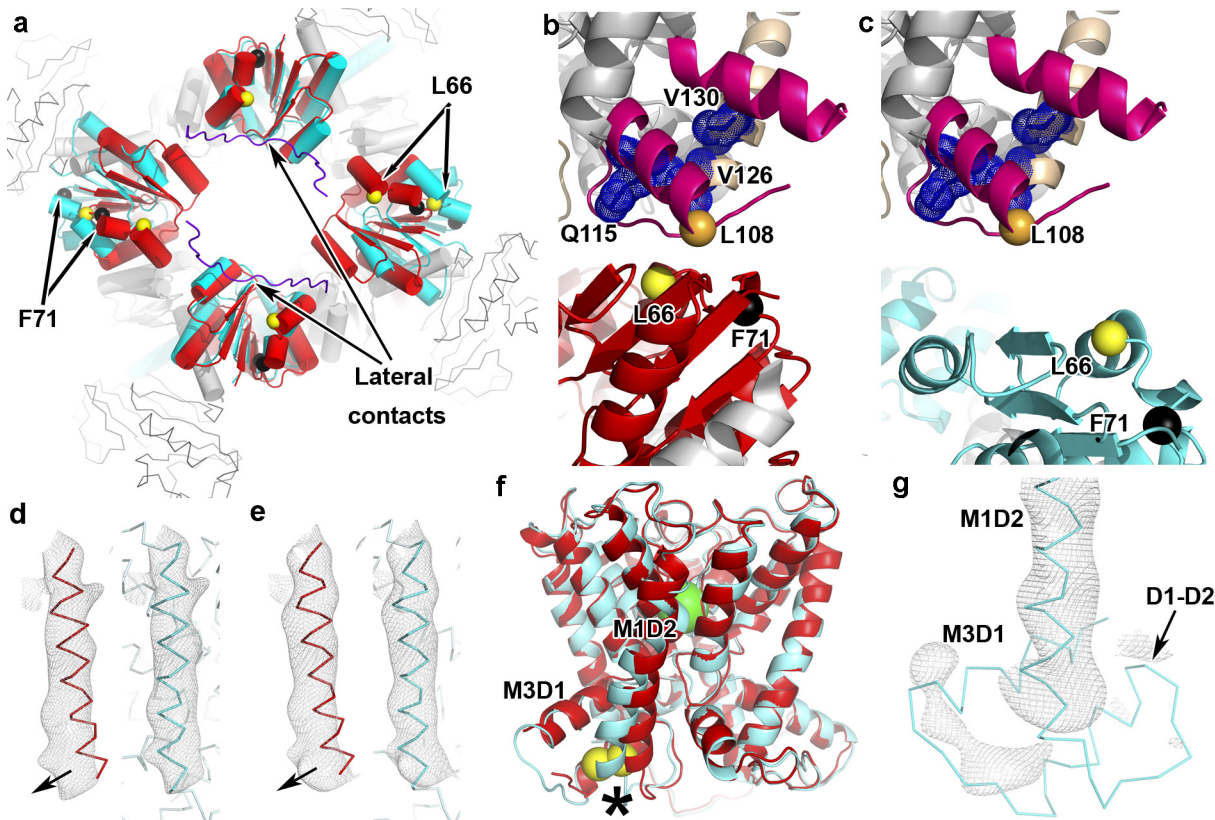


**Fig 2. Comparison of KtrA<sub>ΔC</sub>B-ADP and KtrAB-ATP.** **a**) Face view of RCK rings from KtrA<sub>ΔC</sub>B-ADP (cyan) and KtrAB-ATP (red) superposed through KtrB homodimers; lateral contacts indicated with KtrB C terminus in purple coil. After superposition of KtrA<sub>ΔC</sub>B-ADP and KtrAB-ATP, a D1-D2 domain from KtrAB-ATP (colored magenta and wheat) is shown together with a KtrA subunit from **b**) KtrAB-ATP (red and grey) and **c**) KtrA<sub>ΔC</sub>B-ADP (cyan). Q115, V126, and V130 are shown in dark blue dot representation; C $\alpha$  atoms of L66, F71, and L108 shown as spheres. **d**) and **e**) Averaged density (mesh) of M1D2 helix in two different KtrB subunits. KtrAB-ATP M1D2 helices are shown in red (on the left), and KtrA<sub>ΔC</sub>B-ADP M1D2 helices are in cyan (on the right). Arrow indicates shift applied to cytosolic end of helix to bring into density. **f**) Overall view of superposed KtrB subunits from KtrA<sub>ΔC</sub>B-ADP (cyan) and KtrAB-ATP (red). Star indicates moved M1D2 helix; I127 C $\alpha$  in the two structures is shown as yellow sphere; K<sup>+</sup> ion as green sphere. **g**) Averaged density (mesh) of D1-D2 domain region together with refined KtrA<sub>ΔC</sub>B-ADP model. Lack of density for M3D1 and D1-D2 helices is apparent.

doi:10.1371/journal.pbio.1002356.g002

refinement (S6 Fig). Map quality is relatively poor due to the low resolution of the data and limited averaging power, and caution must be exerted during interpretation. In any case, the density supports our conclusion that the KtrA<sub>ΔC</sub>B-ADP and KtrAB-ADP structures are similar, with density that matches the conformation of the KtrA<sub>ΔC</sub> ring and new density that appears to correspond to the C-terminal domains of full-length KtrA.

The overall organization of KtrA<sub>ΔC</sub>B-ADP and KtrAB-ATP, including the relative disposition of the KtrB homodimer subunits, is similar (Fig 1D–1E). Importantly, the KtrA<sub>ΔC</sub> ring is asymmetrically expanded along the diagonal defined by the tip contacts (Fig 2A), revealing that in the KtrAB complex the ligand-dependent conformational change of the RCK ring occurs along the tip contacts. As a consequence of this change, the KtrB-KtrA interface contact sites are affected differently. In the lateral contacts, the spatial relationship between the KtrB C termini and two KtrA subunits is almost unaltered. The C $\alpha$ -C $\alpha$  distance separating F71 (or L66) in the two lateral contact KtrA subunits is almost unchanged: ~66 and ~65 Å for F71, ~48 and ~49 Å for L66, in KtrAB-ATP and KtrA<sub>ΔC</sub>B-ADP respectively. In the tip contact KtrA subunits, the C $\alpha$ -C $\alpha$  distance F71 distance increases from ~68 Å (KtrAB-ATP) to ~87 Å (KtrA<sub>ΔC</sub>B-ADP), and for L66, from ~50 to ~76 Å. This expansion also includes a KtrA movement away from the membrane protein (Fig 2B and 2C); the distance separating a reference spatial

position (the C $\alpha$  atom of KtrB-L108 in KtrAB-ATP) from the C $\alpha$  of KtrA-F71 increases from ~9 Å in KtrAB-ATP to ~21 Å in KtrA $\Delta$ C-B-ADP.

Although the overall conformations of the KtrA $\Delta$ C ring and isolated KtrA-ADP ring [5] resemble each other, with one diagonal of the ring longer than the other, they are different structures (S7A Fig). This is clearly seen in the C $\alpha$ -C $\alpha$  distances between F71 residues in opposing ring subunits. In the isolated KtrA-ADP structure, these distances are ~68 and ~82 Å, while in KtrA $\Delta$ C from KtrA $\Delta$ C-B-ADP the distances are ~66 and ~87 Å. The intradimer arrangement in KtrA $\Delta$ C-B-ADP is also different from the one seen in the isolated full-length KtrA-ADP structure (S7B Fig); the angle between the KtrA dimer subunits in KtrA $\Delta$ C-B-ADP has changed by ~15° relative to KtrA-ADP. In any case, the angle difference between KtrA $\Delta$ C and KtrA in KtrAB-ATP is even larger, being close to 30° (S7C Fig).

Importantly, the averaged electron-density map also reveals structural changes in the KtrB protein. As in the KtrA ring, all apparent changes are centered on the KtrB tip contact region, and no alterations are detected around the lateral contact. The position of the cytosolic end of the M1 transmembrane helix in repeat D2 (M1D2) in the averaged density is clearly different from the one seen in the KtrAB-ATP structure (Fig 2D and 2E and S8 Fig); the need for a positional adjustment of the helix is also detectable in a difference map (S9 Fig). The M1D2 helix was adjusted with an outward movement of the cytosolic end so that the C $\alpha$  atom of I127 is shifted by ~3–4 Å (Fig 2D–2F). The better fit of the final model to the averaged electron-density map (Fig 2D–2E and S8 Fig) is supported by an increase in the map correlation coefficient calculated for the main chain and C $\beta$  atoms of the cytosolic half of the M1D2 helices (residues 128 to 140) in the 4 KtrB asymmetric unit copies: 0.50 in KtrAB-ATP and 0.71 in KtrA $\Delta$ C-B-ADP. As a result of this conformational change, the M1D2 helix in KtrA $\Delta$ C-B-ADP has been straightened while in KtrAB-ATP it is bent towards the cytosolic pore. In addition, while all other KtrB helices are visible in the averaged electron-density map (including the pore helices and the M3 helices of repeats D2, D3, and D4), there is no density for the two helices just before M1D2, M3D1, and the D1-D2 loop helix (Fig 2G); in KtrAB-ATP, these two helices, together with M1D2, form a domain-like structure (the D1-D2 domain) that functions as a KtrB foot on the tip contact (Fig 1D and 1E). The lack of density for the M3D1 and D1-D2 helices in the 6Å resolution KtrA $\Delta$ C-B-ADP averaged map probably results from either unwinding of the helices, as a manifestation of increased local disorder, or from a breakdown of the KtrB “homodimer” symmetry in this region.

## Remodeling of the Tip-Contact Region during Activation

To explore in more detail the ligand-dependent remodeling of the D1-D2 domain in KtrB, we evaluated the ligand-dependent accessibility of cysteine residues introduced in the D1-D2 domain. We engineered single-cysteine mutations in a cysteineless KtrB (Fig 2B and 2C): Q115C is a semiburied residue on the D1-D2 loop; V126C and V130C are on the M1D2 helix and are semi- (V126C) or fully buried (V130C). These mutants were assembled with cysteineless KtrA (KtrA $\Delta$ C<sub>0</sub>), and we confirmed that the properties of the mutant complexes are similar to wild type KtrAB (S10 Fig): by size-exclusion chromatography, we verified that the complexes are assembled in the presence of ATP and ADP and, using the <sup>86</sup>Rb<sup>+</sup> flux assay, we verified that the mechanism of ligand activation (stimulation by ATP relative to ADP) is not markedly altered. Using a fast injection system, we mixed the complex with ~20-fold molar excess DTNB (5,5'-dithio-bis(2-nitrobenzoic acid)) in the presence of ATP or ADP and followed the reaction time course. DTNB, or Ellman's reagent, reacts rapidly with reduced thiols in tissues and proteins [27–29] and irreversibly in our experimental conditions, generating stoichiometric amounts of the yellow thio-nitrobenzoate (TNB), which absorbs at 412 nm.

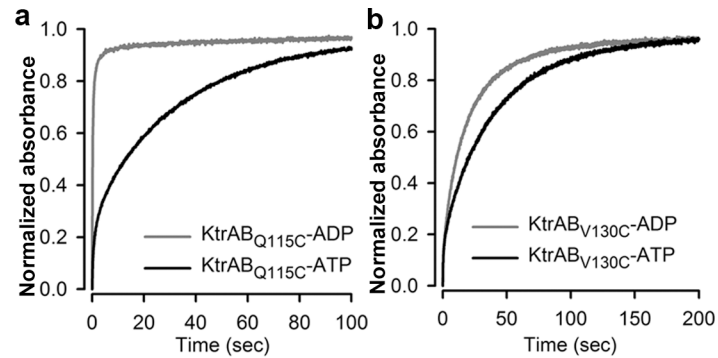


**Fig 3. Remodeling of the tip contact.** Time course of DTNB modification reaction for **a)** KtrAB<sub>Q115C</sub> and **b)** KtrAB<sub>V130C</sub> in complex with KtrA<sub>C0</sub> bound to ADP (gray) or ATP (black). Representatives of four separate modification reactions are shown, normalized to maximum (last recorded) value. For each mutant, the final absorption values between ADP and ATP varied by less than 30%, showing that differences in initial cysteine oxidation levels are small. The initial fast jump observed in the time course is due to the time resolution of our system (100 ms). Numerical values are included in [S1 Data](#).

doi:10.1371/journal.pbio.1002356.g003

The DTNB modification time courses for Q115C ([Fig 3A](#)) clearly show that the reaction is much faster (~65 times faster) in the presence of ADP than in the presence of ATP; the modification halftimes are ~0.2 sec and ~13 sec with ADP and ATP, respectively ([Table 1](#)). With the KtrAB<sub>V126C</sub> mutant, the reactions are remarkably fast in the presence of either ligand, and we cannot detect a difference in reactivity ([Table 1](#), [S10B Fig](#)), but the modification half-time for KtrAB<sub>V130C</sub> (~10 s) is also shorter for ADP than with ATP (~21 s) ([Fig 3B](#) and [Table 1](#)). Faster reaction time courses for ADP relative to ATP for two different cysteine positions in the D1-D2 domain are consistent with an increase in cysteine accessibility to DTNB in the ADP-bound state and support the proposal that the domain has undergone a structural change. This biochemical analysis together with our structural comparison establishes that during ligand activation the RCK ring conformational change is associated with remodeling of the tip contact interface and D1-D2 domain.

### The KtrB Cytosolic Pore Becomes Narrower during Activation

A central feature of the activation mechanism of many K<sup>+</sup> channels is the opening of a cytoplasmic gate and increased access to the cytosolic pore. Since Trk/Ktr/HKT proteins are

**Table 1. DTNB modification reaction halftimes for mutant cysteines.**

	ADP (s)	ATP (s)
<b>Cysteines introduced in the D1-D2 domain</b>		
Q115C	0.23 ± 0.01	12.75 ± 0.48
V126C	0.21 ± 0.01	0.21 ± 0.02
V130C	10.48 ± 0.09	20.95 ± 0.39
<b>Cysteines introduced in the cytosolic pore</b>		
N119C	0.24 ± 0.01	0.55 ± 0.01
P121C	0.23 ± 0.02	0.91 ± 0.05
F443C	0.48 ± 0.01	63.73 ± 0.43
T444C	52.43 ± 4.02	386.55 ± 106.99 *

SEM values are determined from 3–4 separate modification reactions.

\* Halftime for T444C with ATP is underestimated since the reaction is very slow and does not reach its end point.

doi:10.1371/journal.pbio.1002356.t001

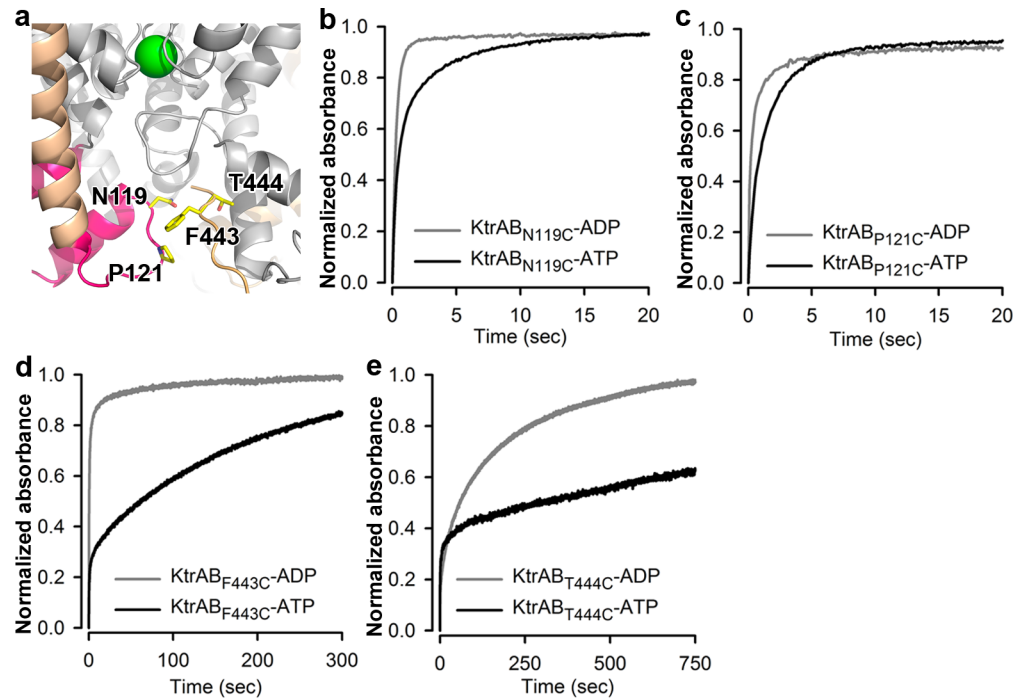


**Fig 4. Narrowing of cytosolic pore.** **a**) View of cytosolic pore wall residues (in yellow stick) that were mutated to cysteines. KtrB C-terminus shown as orange coil; D1-D2 domain from KtrAB-ATP shown in magenta and wheat;  $K^+$  ion as green sphere. Time course of DTNB modification reaction for **b**) KtrB<sub>N119C</sub>, **c**) KtrB<sub>P121C</sub>, **d**) KtrB<sub>F443C</sub> and **e**) KtrB<sub>T444C</sub> in complex with KtrA<sub>C0</sub> bound to ADP (gray) or ATP (black). Representatives of four separate modification reactions are shown. Normalized to maximum (last recorded) value. The initial fast jump in the time course (very noticeable in ATP time courses of F443C and T444C) is due to the time resolution of our system (100 ms). For N119C, P121C, and F443C, the final absorption values between ADP and ATP varied by less than 30%, showing that differences in cysteine oxidation are small; this value could not be determined for T444C with ATP due to its very slow reactivity. Numerical values of data displayed in panels b–e are included in [S1 Data](#).

doi:10.1371/journal.pbio.1002356.g004

structurally similar to  $K^+$  channels, we asked whether the same happens in KtrAB during activation. To assess the ligand-dependent conformational changes in the pore of KtrB, we made use of the DTNB assay (introduced above) and probed ligand-induced changes in accessibility of cysteine residues introduced on the wall of the cytosolic pore of KtrB. In the KtrAB-ATP structure, N119C is positioned at the mouth of the pore, while P121C, F443C, and T444C are positioned deep in the pore (Fig 4A). These mutants showed no alteration in their ability to assemble with KtrA and retained the ATP stimulation effect, although reduced for F443C (S11 Fig).

The DTNB modification halftimes measured for the four cysteine mutants were consistently shorter with ADP than with ATP (Fig 4B–4E, Table 1), showing that all cysteine thiol groups are less reactive in the ATP-bound state. This trend across four different positions strongly indicates a reduction in DTNB accessibility. These results, together with the ligand-dependent repositioning of the M1D2 helix towards the cytosolic pore in KtrAB-ATP (Fig 2F), suggest that the cytosolic pore of KtrAB becomes narrower upon ATP activation.

## Functional and Biochemical Characterization of the Intramembrane Gate

The intramembrane loop and the conserved arginine are thought to function as a gate in KtrAB and TrkHA. We analyzed the functional impact of mutations both in the loop and in



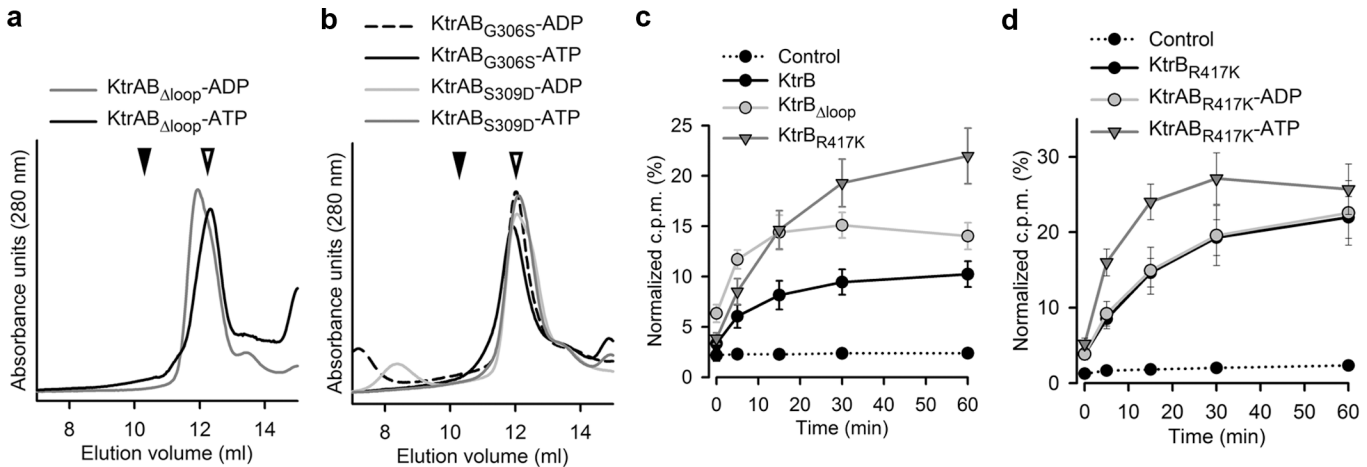


**Fig 5. Properties of intramembrane gate mutants.** Size-exclusion profiles of intramembrane loop **a)** truncation and **b)** G306S and S309D single mutants assembled with KtrA in the presence of ATP and ADP. Inverted arrow heads indicate elution volumes of KtrAB complex (closed symbol) and of separate components (open symbol). SDS-PAGE of fractions are shown in [S12 Fig](#); **c)** Time course of  $^{86}\text{Rb}^+$  uptake for KtrB wt and mutants (KtrB $_{\Delta\text{loop}}$ , KtrB $_{\text{R417K}}$ ) in the absence of KtrA. **d)** Time course of  $^{86}\text{Rb}^+$  uptake for KtrB $_{\text{R417K}}$  alone and KtrAB $_{\text{R417K}}$  with ADP or ATP. Liposome float-up experiments are shown in [S13 Fig](#). Numerical values of data displayed in panels c–d are included in [S1 Data](#).

doi:10.1371/journal.pbio.1002356.g005

the arginine (R417). We truncated the intramembrane loop (KtrB $_{\Delta\text{loop}}$ —truncation of residues G306 to A311), mutated two residues in the loop (KtrB $_{\text{G306S}}$  and KtrB $_{\text{S309D}}$ ), and mutated the conserved arginine to a lysine (KtrB $_{\text{R417K}}$ ). Strikingly, the intramembrane loop seems to be very sensitive to alterations since both the truncation ([Fig 5A](#)) and the two single point mutations ([Fig 5B](#)) have a destabilizing effect on the interaction between KtrB and KtrA. Hanelt and colleagues [21] described the same effect for truncations of the intramembrane loop in *V. alginolyticus* KtrB but did not observe destabilization with a mutation equivalent to G306S. In contrast, KtrB $_{\text{R417K}}$  assembles with KtrA ([S2B Fig](#)) in the presence of ADP or ATP.

Flux assays with liposome-reconstituted KtrB $_{\Delta\text{loop}}$  and KtrB $_{\text{R417K}}$  show that the uptake in KtrB $_{\Delta\text{loop}}$  is faster than in the KtrB wild type protein (single exponential time constants  $[\tau]$  are  $\sim 5$  min for KtrB $_{\Delta\text{loop}}$  and  $\sim 11$  min for wild type KtrB) as expected if an obstacle to ion flow has been removed ([Fig 5C](#)). On the other hand, the rate of uptake in KtrB $_{\text{R417K}}$  alone ( $\tau \sim 22$  min) is slow. More interestingly, the uptake rate of KtrAB $_{\text{R417K}}$ -ATP ( $\tau \sim 6$  min) is as fast as in KtrB $_{\Delta\text{loop}}$  ([Fig 5D](#)) while KtrAB $_{\text{R417K}}$ -ADP ( $\tau \sim 22$  min) is comparable to wild type KtrAB ( $\tau \sim 19$  and  $\sim 17$  min, for KtrAB-ATP and KtrAB-ADP respectively). This suggests that the conservative substitution in the KtrAB $_{\text{R417K}}$  complex is functionally similar to the removal of the intramembrane loop from the cytosolic pore of KtrB. Note however that this effect is ligand-dependent since it only occurs when KtrB $_{\text{R417K}}$  is associated with KtrA with bound ATP and not with ADP.

Overall, changes in the intramembrane loop or in R417 modify the ion permeation properties in a way that is consistent with a role in the intramembrane gate.

## Discussion

The structures of the isolated RCK rings from the KtrAB and TrkHA ion transporters led to the proposal that ligand-induced conformational changes in the RCK rings (KtrA or TrkA) are at the basis of the activation mechanisms of the Ktr and Trk ion transporters [5,8,18]. In KtrAB in particular, it was shown that the isolated KtrA ring expands asymmetrically upon exchange of ATP for ADP. However, those studies did not show how the asymmetric expansion/contraction occurs within the complex. In fact, no conformational changes had been demonstrated in the KtrAB and TrkHA complexes.

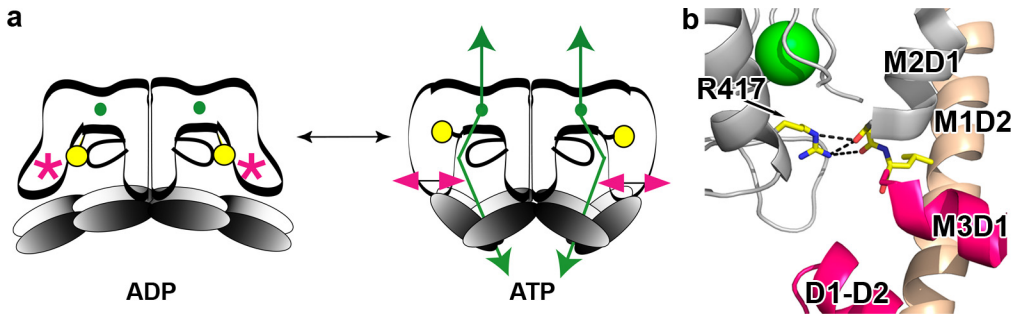


**Fig 6. Proposed mechanism of activation in KtrAB.** **a)** Model for KtrAB ligand activation: ion flux stimulation by ATP (green arrows) results from a change in the conformation of the RCK ring (gray ovals) and D1-D2 domain (magenta arrows). These changes alter the interactions established by R417 (yellow circle) with the D1-D2 domain (magenta star). **b)** View of R417 side chain in KtrAB-ATP structure establishing contacts with main chain carbonyls in the C-terminus of M2D1 helix. K<sup>+</sup> ion as green sphere; helices are labeled.

doi:10.1371/journal.pbio.1002356.g006

We have now presented structural, biochemical, and functional evidence establishing that KtrAB activation by ATP involves a ligand-dependent asymmetrical contraction of the KtrA gating ring, changes in the tip contact interface and remodeling of the D1-D2 domain (Fig 6A).

Our results also reinforce the notion that the intramembrane loop and the conserved arginine (R417) form the gate in KtrAB and TrkHA [18,20–22,30] (see S1C Fig). Destabilization of the interaction between KtrB and KtrA that results from intramembrane loop modifications appears to be more consistent with the loop having a structural role than being a mobile component of a gate. Our work brings forth the functional importance of R417 in the activation mechanism; the conservative mutation R417K in the KtrAB<sub>R417K</sub> complex is functionally similar to removing six residues from the intramembrane loop, resulting in an increased rate of ion flux; strikingly, this functional effect is ligand-dependent, since in KtrAB<sub>R417K</sub> the increase in the rate of flux is only observed with ATP. The importance of R417 in the activation mechanism is further reinforced by inspection of the KtrAB-ATP structure. This residue interacts with the main chain carbonyls at the C-terminal end of the M2D1 helix (Fig 6B), a helix that is directly connected to and abuts the D1-D2 domain. It is thus possible to envisage that contraction/expansion of the KtrA ring and rearrangements of the tip contact region and D1-D2 domain will alter the interactions between R417 and the C-terminal end of the M2D1 helix, affecting therefore the intramembrane gate (Fig 6A).

Block of the ion permeation pathway by the intramembrane gate in the KtrAB-ATP structure [5] remains a puzzle. One possibility is that in detergent, the ion transporter is not able to adopt the fully activated conformation. Another possibility is that ATP binding is connected to several different conformations, and in the KtrAB-ATP structure, we captured a conformation where the intramembrane gate blocks the pathway, not unlike the desensitized state of some ligand-gated ion channels [31–34].

A remarkable aspect of the ligand-dependent mechanism of activation in KtrAB that has been revealed by our data is that the KtrA ring (an RCK ring) contracts, and the KtrB cytosolic pore narrows down with activation. This is very different from what happens in the related MthK or BK potassium channels that are also regulated by ligand binding to their RCK rings. In these channels, binding of the activating ligand (Ca<sup>2+</sup>) to the RCK ring results in an expansion of the ring and widening of the cytosolic pore [15,35,36]. Moreover, activation in the majority of K<sup>+</sup> channels results in increased accessibility to the cytosolic ion pore [37–40]. An explanation for this apparently contradictory result is found in the KtrAB-ATP structure. It shows that, despite narrowing of the pore, there is a water-accessible conduit up to the intramembrane gate. It is therefore likely that narrowing of the cytosolic pore during activation

results from the reorganization of a long-range allosteric network that has to connect the tip contact (and the RCK ring) and the intramembrane gate. Upon ATP activation, the cytosolic pore narrows down but remains wide enough to allow easy permeation of fully or partially solvated potassium ions.

In summary, despite the structural similarity to K<sup>+</sup> channels, the mechanisms of ligand activation in Trk/Ktr/HKT ion transporters are unique.

## Materials and Methods

### Protein Expression and Purification

N-terminal His-tagged KtrB (GenBank: KIX81591.1) cloned in a modified pET-24d vector (Novagen) was overexpressed in *Escherichia coli* BL21(DE3). Cells grown in LB media at 37°C were induced with 0.5 mM IPTG for 2.5 h. Cells were lysed in protease inhibitor-supplemented buffer (50 mM Tris-HCl pH 8.0, 120 mM NaCl, 30 mM KCl) and KtrB extracted with 40 mM DDM (*n*-dodecyl- $\beta$ -D-maltoside, solgrade from Anatrace) overnight at 4°C. Spin-cleared lysate was loaded into a Talon metal affinity resin (Clontech) and washed with 50 mM Tris-HCl pH 8.0, 270 mM NaCl, 30 mM KCl, 1 mM DDM followed by buffer A (50 mM Tris-HCl pH 8.0, 120 mM NaCl, 30 mM KCl, 1 mM DDM) supplemented with 20 mM imidazole. Protein was eluted with buffer A supplemented with 150 mM imidazole and immediately 3-fold diluted in buffer A supplemented with 15 mM DTT and 1.5 mM TCEP. Eluted fractions were concentrated to ~2.5 mg/ml and incubated overnight at 4°C with thrombin for tag cleavage. At this point, the protein was either assembled with KtrA (for protein crystallography) or further purified by size exclusion with a Superdex-200 column.

Wild type KtrA (GenBank: KIX81590.1) and cysteine-less KtrA (KtrA<sub>C0</sub>—C22V, C178V, C109S, C204S) were overexpressed in *E. coli* BL21(DE3), grown in LB media at 20°C, after ~14–16 h induction with IPTG. Cells were lysed in 50 mM Tris-HCl pH 7.5, 50 mM KCl, 5 mM DTT, and the spin-cleared lysate was loaded into an anion exchange column. KCl gradient-eluted fractions containing KtrA were pooled and incubated with ADP-agarose resin (Innova Biosciences) overnight at 4°C. Beads were washed thoroughly with Buffer B (50 mM Tris-HCl pH 8.0, 150 mM KCl, 1 mM TCEP), and protein was eluted in buffer B supplemented with either 5 mM ADP or ATP (sodium salts). Protein was concentrated to ~3 mg/ml and further purified by size exclusion with a Superdex-S200 column using buffer C (50 mM Tris-HCl pH 7.5, 150 mM KCl, 5 mM DTT). KtrA in solution was supplemented with 1 mM adenine-nucleotide from a 100 mM stock in 1 M Tris-HCl pH 7.5.

The KtrA<sub>ΔC</sub> construct includes two N-terminal KtrA domains in tandem (residues 1–144 + 7–144), connected by a linker (-LEGS-), and cloned in a modified pET-24d vector (Novagen). This tandem protein does not aggregate as easily as a single N-terminal KtrA domain. Purification of KtrA<sub>ΔC</sub> followed the procedure described before [11]. Briefly, the protein was overexpressed in BL21(DE3) by overnight induction at 20°C; cell lysate in buffer D (50 mM Tris-HCl pH 8.5, 120 mM NaCl, 30 mM KCl) was loaded into a His-tag affinity column, and protein was eluted with buffer supplemented with 150 mM Imidazole; after adding thrombin for cleavage of tag, protein was dialysed overnight at 4°C against buffer D supplemented with 5 mM DTT; protein was concentrated and further purified in a size-exclusion Superdex-200 column with 20 mM Tris pH 8.5, 150 mM NaCl, 5 mM DTT before assembling with KtrB.

For protein crystallography, the KtrA<sub>ΔC</sub>B-ADP and KtrAB-ADP were prepared by mixing purified KtrB with an excess of pure KtrA<sub>ΔC</sub> or KtrA. The mixture was concentrated and purified in a size-exclusion Superdex-200 column with 20 mM Tris-HCl pH 8.0, 120 mM NaCl, 30 mM KCl, 5 mM DTT, 1.5 mM 6-cyclohexyl-1-hexyl- $\beta$ -D-maltoside (cymal-6, anagrade, from Anatrace). Collected fractions were concentrated to 7–10 mg/ml after adding ADP to 1 mM.

For biochemical experiments, size-exclusion purified KtrB (wild type or cysteine mutants) was mixed with an excess of KtrA (wild type, KtrA<sub>C0</sub> or KtrA<sub>ΔC</sub>) and directly used in the assays. For DTNB modification assays, KtrA<sub>C0</sub> was prepared in the absence of DTT and TCEP throughout the complete purification procedure to avoid cross reaction of DTNB with the reducing agent.

## Crystallization

KtrA<sub>ΔC</sub>B was crystallized by mixing 1 μl of protein complex at ~10 mg/ml with 1 μl of crystallization solution (100 mM Tris-HCl pH 8.5, 18%–22% PEG400, 100–200 mM CaCl<sub>2</sub>) and incubating at 20°C. Crystals were cryoprotected by increasing PEG400 to 29% by adding directly to drop from 45% stock, equilibrating for 2 d, and then mixing cryosolution (45% PEG400, 250 mM CaCl<sub>2</sub>, 15 mM cymal-6, 100 mM Tris-HCl 8.5) before dropping crystal into liquid nitrogen. KtrAB-ADP was crystallized by mixing 1 μl of protein complex at ~7 mg/ml with 1 μl of crystallization solution (100 mM Hepes pH 7.5, 1 M NaCl, 10% PEG4000) and incubating at 20°C. Crystals were cryoprotected by transferring sequentially to 100 mM Hepes pH 7.5, 25% PEG4000, 1 M NaCl, 1.5 mM cymal-6, 0.5 mM ADP with 10% glycerol, and to the same solution with 25% glycerol, before dropping crystal into liquid nitrogen.

## Data Processing and Structure Determination

Diffraction data from KtrA<sub>ΔC</sub>B-ADP crystals were collected at Soleil Proxima 2 and from KtrAB-ADP at ESRF ID14-4 and processed with XDS [41]. KtrA<sub>ΔC</sub>B-ADP structure was solved by molecular replacement with PHASER (CCP4 package [42]) using the KtrB dimer from KtrAB-ATP (PDB 4J7C) and the KtrA octameric ring (without C-terminal domain) (PDB 2HMS). 4-fold (around KtrB) and 8-fold (around KtrA<sub>ΔC</sub>) averaging was performed using DMmulti (CCP4 package [42]) with masks calculated with MAMA. Rigid body refinement of KtrA<sub>ΔC</sub>B was performed with PHENIX [43] using a single data bin and 12 groups (1 for each of the KtrA<sub>ΔC</sub> and KtrB subunits). DEN-refinement [44] was performed using SBGrid Science Portal server (<https://portal.sbgrid.org/d/apps/den>) using a single overall B-factor (no group or individual B-factor refinement), restrained NCS (two groups, corresponding to KtrA<sub>ΔC</sub> and KtrB, and restraining weight of 300), no positional refinement, DEN restraints with 3–15 Å cutoff, and no sequence or chain separation limits. Combinations of starting annealing temperatures,  $W_{DEN}$  and  $\gamma$  factor were tested, and the best solution, as a combination of Ramachandran plot and  $R_{free}$ , was obtained with annealing temperature of 3,000 K,  $W_{DEN} = 300$  and  $\gamma = 1.0$ . Lowest  $R_{free}$  solution differed by 0.23% in  $R_{free}$  from selected coordinates but presented much worse stereochemistry (only 67% of residues in the favored region of a Ramachandran plot).

## Preparation of Proteoliposomes

Proteoliposomes were prepared as previously described [5] with modifications. Polar *E. coli* lipids (Avanti) in chloroform were dried under a stream of argon. Residual solvent was removed by pentane wash and redrying of the film. Lipids were resuspended at 10 mg/ml in swelling buffer (150 mM KCl, 10 mM Hepes, 5 mM N-methylglucamine, pH 7.4) using a bath sonicator. Lipids were solubilized by adding 40 mM decylmaltoside (solgrade from Anatrace) from powder and left for ~2 h with gentle agitation at room temperature. KtrAB complex was prepared and dialyzed overnight at 4°C prior against 150 mM KCl, 10 mM Hepes, 5 mM N-methylglucamine, 5 mM DTT, 0.5 mM DDM, pH 7.4, with nucleotide. Adenine nucleotide levels were adjusted during dialysis to spontaneously reach 20 μM after reconstitution (calculated from protein concentration and the corresponding dilution factor [volume added to lipid

aliquots]). Protein was added to solubilized lipids at 1:100 (w:w) protein-to-lipid ratio and incubated for 30 min at room temperature. The amount of protein added to 100  $\mu$ l aliquot of lipids was adjusted to contain 10  $\mu$ g KtrB both when reconstituted alone or as KtrAB complex. Detergent was removed by adsorbing SM-2 Biobeads (BioRad): the protein-lipid mix was incubated twice with fresh BioBeads at 10:1 (w:w) bead-to-detergent ratio at room temperature for 1 h, followed by an overnight incubation at 4°C at a 20:1 (w:w) bead-to-detergent ratio. Control liposomes were prepared similarly, except that only KtrA (wt, KtrA<sub>C0</sub> or KtrA<sub>ΔC</sub>) was added to the solubilized lipids.

### <sup>86</sup>Rb<sup>+</sup> Flux Assay

Assay was performed as previously described [5] with small modifications. A K<sup>+</sup> gradient was formed by spinning 100  $\mu$ l aliquot of liposomes through a 1.5 ml bed of Sephadex G50 (fine) preswollen in sorbitol buffer (20  $\mu$ M KCl, 150 mM sorbitol, 10 mM Hepes, 5 mM N-methylglucamine, pH 7.4) and supplemented with 20  $\mu$ M adenine nucleotide. Liposomes were then mixed with twice the volume of <sup>86</sup>Rb<sup>+</sup> assay buffer (<sup>86</sup>Rb<sup>+</sup> at ~2,000 counts/ $\mu$ l in sorbitol buffer) and the reaction was run for 60 min. At selected time points, 100  $\mu$ l aliquots of uptake reactions were loaded into Dowex cation exchange columns (prewashed in 150 mM sorbitol solution plus 5 mg/ml bovine serum albumin and pre-equilibrated in 150 mM sorbitol solution) and eluted with 6% sorbitol solution. The eluate (liposomes with accumulated <sup>86</sup>Rb<sup>+</sup>) was collected in 4 ml scintillation vials and mixed with Optiphase scintillation fluid at 1:1 (v:v). At the end of each experiment (at 60 min), valinomycin was added to the last 100  $\mu$ l aliquot of the uptake reaction at a final concentration of 900 nM, incubated for 6 min and then loaded into Dowex columns as described above. The uptake of <sup>86</sup>Rb<sup>+</sup> into liposomes was expressed as the percentage of the counts measured after valinomycin treatment (this step corrects for reconstitution variability among different batches of liposomes).

In detergent, both KtrB and TrkH associate with the respective RCK ring partners as either one membrane-protein dimer or as two dimers, with each dimer binding to opposite faces of the ring (see S4 Fig) [5,18]. To favor the formation of the complex with one KtrB dimer plus one KtrA octamer, we performed the liposome reconstitution with a fixed amount of KtrB and an excess of KtrA or KtrA<sub>ΔC</sub>. Any unforeseen effect of the free KtrA or KtrA<sub>ΔC</sub> protein fraction on the liposomes was controlled by reconstituting liposomes with KtrA or KtrA<sub>ΔC</sub> alone. These liposomes are used to evaluate the background signal of the assay; it is however important to realize that the fraction of free regulatory protein in the KtrAB or KtrA<sub>ΔC</sub>B reconstituted liposomes is much lower than in these background liposomes since most of the protein will be present in a membrane protein complex.

The increased background signal observed in the KtrA<sub>ΔC</sub>B flux assay results from a reduction in the radioactivity uptake observed with valinomycin flux in the KtrA<sub>ΔC</sub> liposomes. Since valinomycin values are used for normalization of the assay, smaller valinomycin values for KtrA<sub>ΔC</sub> liposomes result in normalized flux uptake that is larger than for full-length KtrA-liposomes. Valinomycin flux reduction is consistent with increased leakiness of the KtrA<sub>ΔC</sub> liposomes; leakiness in the KtrA<sub>ΔC</sub> liposomes decreases the electrical potential gradient in these liposomes and lowers the uptake of <sup>86</sup>Rb<sup>+</sup>. The molecular basis for this effect is not known. As stated in the previous paragraph, leakiness would be more pronounced in the KtrA<sub>ΔC</sub>-liposomes since the amount of free KtrA<sub>ΔC</sub> protein is higher in control liposomes than in KtrA<sub>ΔC</sub>B liposomes.

### Liposome Float-Up Experiments

50  $\mu$ l of proteoliposomes in 40% (w/v) sucrose were put into the bottom of polyallomer centrifuge tubes (Beckman Coulter) and sequentially overlaid with 100  $\mu$ l of 20% sucrose solution

and 50  $\mu$ l of 5% sucrose solution, forming a discontinuous gradient from bottom to top. The samples were centrifuged at 100,000  $g$  for 60 min at 4°C in an Airfuge Ultracentrifuge (Beckman Coulter) using the A-100/18 rotor. Fractions of 40  $\mu$ l each were collected from top to bottom and protein was detected by western blotting.

Samples were run in 10% or 15% polyacrylamide gel, blotted onto nitrocellulose membrane, and probed with anti-KtrB polyclonal antibody (overnight incubation at 4°C) or anti-KtrA polyclonal antibody (2 h at room temperature), respectively. Detection was done by incubation with anti-rabbit IgG conjugated with peroxidase (Sigma) for 30 min at room temperature and using Amersham ECL Prime western blotting detection reagents.

## Cysteine Modification with DTNB

Just prior to initiating the DTNB modification reaction, KtrB in DTNB buffer (20 mM Tris-HCl pH 8.0, 120 mM NaCl, 30 mM KCl, 5 mM EDTA, 0.5 mM DDM) was mixed with excess of KtrA<sub>CO</sub> in buffer C without DTT while keeping the detergent concentration well above its critical micellar concentration. For each reaction KtrB was present at a concentration of 14–20  $\mu$ M KtrB. The protein was loaded into one input channel of a rapid mixing device (SFA-20 Rapid Kinetics Accessories, Hi-TECH, TgK Scientific). The second channel was loaded with 400  $\mu$ M DTNB dissolved in DTNB buffer. Solutions were mixed upon manual injection into the flow cell, which was placed in the cuvette holder of a Shimadzu UV-2401 spectrophotometer. As a result of the 1:1 mixing of protein and reagent, the final concentration of the reactants is halved. DTNB is a water-soluble compound and partitions weakly into detergent micelles, which makes it an ideal candidate for our experiments with a detergent-solubilized membrane protein. The release of TNB from DTNB was followed at 412 nm with 1 nm open slit with 10 points/sec sampling rate. Before each assay, we filled the flow cell with DTNB and blanked the system to eliminate any background signal.

With ~20-fold molar excess of DTNB over protein and in the absence of reducing agents, we were expecting to observe an apparent first order reaction. Instead, we consistently observed multiple components in the modification time course. Control experiments with reduced glutathione and DTNB (both in the presence and absence of 0.5 mM DDM) showed a first-order reaction demonstrating that the multiple components seen with the membrane protein were not the result of our experimental setup or the presence of detergent. Fitting the time course with multiple exponentials revealed that one exponential component dominated with an amplitude of at least 70%. We concluded that the complex reaction kinetics are a feature of protein modification with DTNB that result from the natural existence of population variability. In any case, instead of using a mean time constant obtained from a multiple exponential fit to describe the time course, we used the reaction half-time. When using sufficiently long experimental recording times, the reaction half-time minimizes the error that results from the presence of a very slow component in the time-course.

Modification of accessible thiols with DTNB produces stoichiometric amounts of TNB, and as a consequence the final absorbance value is defined by the initial concentration of reactive cysteine. Differences between the final absorbance values of a particular mutant with ATP and ADP were less than 70%. Note, that after 1 h incubation of DTNB with unfolded KtrAB protein (mixed with 3 M guanidium-hydrochloride) we obtained ~1 cysteine/KtrB subunit for all tested constructs, as expected.

## Supporting Information

**S1 Data. Numerical values of data displayed in Figs [1A and 1B](#), [3A and 3B](#), [4B–4E](#), [5C and 5D](#), [S10A–S10C](#), and [S11A–S11D](#).**  
(XLSX)

**S1 Fig. Similarities between KtrAB and K<sup>+</sup> channels.** Extracellular views of **a)** KtrB homodimer and **b)** KcsA K<sup>+</sup> channel. Side views of **c)** a single KtrB subunit without the 2nd repeat and **d)** KcsA pore without a channel subunit. Each repeat and subunit is colored a different shade of blue. KtrB repeats are labeled. Transmembrane and pore helices of one repeat or subunit are labeled. The intramembrane loop and conserved arginine are indicated. K<sup>+</sup> are shown as green spheres bound in the selectivity filter. Structure of RCK octameric ring in **e)** KtrA (with a C-terminal domain indicated) and in **f)** MthK K<sup>+</sup> channel. Alternate subunits are shown in red and gray.

(TIF)

**S2 Fig. Assembly of KtrA<sub>ΔC</sub>B and KtrAB<sub>R417K</sub>.** Size-exclusion profiles of **a)** KtrB assembled with KtrA<sub>ΔC</sub> in the presence of ATP and ADP and **b)** KtrB<sub>R417K</sub> mutant assembled with KtrA in the presence of ATP and ADP. Closed inverted arrowhead indicates elution volume of KtrAB complex; open arrowhead indicates elution volume of individual components. SDS-PAGE of size-exclusion fractions are shown as insets. Inset in **a)** 1- KtrB preparation before size exclusion; 2- KtrA<sub>ΔC</sub>+KtrB with ADP eluting at closed arrow; 3- KtrA<sub>ΔC</sub>+KtrB with ADP eluting at open arrow; 4- KtrA<sub>ΔC</sub>+KtrB with ATP eluting at closed arrow; 5- KtrA<sub>ΔC</sub>+KtrB with ATP eluting at open arrow; 6- Pure KtrB. Inset in **b)** 1- Pure KtrB<sub>R417K</sub>; 2- Pure KtrB<sub>R417K</sub>; 3- KtrA+KtrB<sub>R417K</sub> with ADP eluting at closed arrow; 4- KtrA+KtrB<sub>R417K</sub> with ADP eluting at open arrow; 5- KtrA+KtrB<sub>R417K</sub> with ATP eluting at closed arrow; 6- KtrA+KtrB<sub>R417K</sub> with ATP eluting at open arrow. Lower horizontal arrow indicates KtrA<sub>ΔC</sub>-tandem or full-length KtrA; horizontal arrows with M or D indicate KtrB monomer or dimer, respectively

(TIF)

**S3 Fig. Western blots of fractions collected from float-up experiments.** Westerns were probed with anti-KtrB or anti-KtrA antibody. Fractions 1 to 5 correspond to 40 μl fractions collected from low to high sucrose concentration; liposomes float to the low density fractions. KtrB float-up distribution for **a)** KtrAB-ATP and -ADP reconstituted liposomes; or **b)** KtrA<sub>ΔC</sub>-B-ATP and -ADP reconstituted liposomes. The experiments show that reconstituted KtrB is present in fractions 1 and 2 demonstrating that the membrane protein is associated with liposomes. KtrA float-up distribution after external addition of KtrA-ATP or -ADP to preformed **c)** empty liposomes or **d)** KtrB-reconstituted liposomes. Importantly, just like in the flux assay, KtrA was added in excess relative to KtrB. In the liposomes without KtrB (empty liposomes), the KtrA protein is not associated with liposomes and is detected in the high density fractions. When KtrA was added to KtrB liposomes, the protein distribution is changed such that KtrA is detected in all fractions, some is associated with the liposomes, and some is present as free protein in the fractions with a high concentration of sucrose. L indicates sample loaded in float-up, + indicates sample before reconstitution. Horizontal arrows with M or D indicate KtrB monomer or dimer, respectively.

(TIF)

**S4 Fig. Contents of asymmetric unit.** Contents of asymmetric unit in KtrA<sub>ΔC</sub>B crystals are shown, with two KtrB dimers associated with one KtrA<sub>ΔC</sub> ring on opposite faces. Subunits are shown in different colors. Spheres indicate K<sup>+</sup>.

(TIF)

**S5 Fig. Collection of KtrA RCK rings.** RCK rings (without C-terminal domain) used as molecular search models against KtrAB-ADP data from: **a)** full-length KtrA-ATP (model 1—PDB code 4J90); **b)** full-length KtrA-ADP (model 2—PDB code 4J91); **c)** KtrA<sub>ΔC</sub> (model 3—PDB code 2HMS); **d)** KtrA<sub>ΔC</sub> (model 4—PDB code 2HMW); **e)** KtrA<sub>ΔC</sub> (model 5—PDB code

2HMU); f) KtrA<sub>ΔC</sub> from KtrA<sub>ΔC</sub>B structure (model 6 and 7—PDB code 5BUT). F71-C $\alpha$  atoms at each of the subunits are shown as black spheres. Distances between F71 in pairs of opposite subunits are indicated for each ring in Angstroms.

(TIF)

**S6 Fig. Averaged map of KtrAB-ADP.** Averaged map calculated with KtrAB-ADP 8 Å diffraction data and using starting phases calculated from the model 7 molecular replacement solution (S3 Table). Superposed on the map is the KtrB model from KtrA<sub>ΔC</sub>B and the full-length KtrA-ADP structure previously determined. Two KtrB dimers are indicated with density covering one of the dimers. Density covering the N-terminal domain and C-terminal domain (not included in the initial phasing) of two KtrA subunits is also indicated.

(TIF)

**S7 Fig. Comparison of RCK rings in KtrA<sub>ΔC</sub>B and KtrA-ADP.** a) Face view of superposed KtrA-ADP (black C $\alpha$  trace) and KtrA<sub>ΔC</sub> (cyan). F71-C $\alpha$  atoms are shown as cyan and black spheres. Superposition (through one of the N-terminal domains) of KtrA<sub>ΔC</sub> ring dimer (cyan) with dimer from b) KtrA-ADP (black) or c) KtrA-ATP (red) from KtrAB-ATP structure. C-terminal domains are not shown. Angle values referring to the structural changes between RCK ring dimers, and quoted in the main text, were measured between axes of the last  $\alpha$ -helix in the N-terminal domain, as indicated by cyan, black, and red lines.

(TIF)

**S8 Fig. Movement of M1D2 helix.** Averaged density (mesh) of M1D2 helix in two different KtrB subunits. Together with Fig 2D and 2E, these two panels show the averaged density for all M1D2 helices of the 4 KtrB subunits in the asymmetric unit of KtrA<sub>ΔC</sub>B. KtrAB-ATP M1D2 helices are shown in red (on the left) and KtrA<sub>ΔC</sub>B-ADP M1D2 helices are in cyan (on the right). Arrow indicates shift applied to cytosolic end of helix to bring it into density.

(TIF)

**S9 Fig. KtrA<sub>ΔC</sub>B Difference map.** Fo-Fc difference map calculated with structure factors from KtrA<sub>ΔC</sub>B dataset and structure factors and phases from molecular replacement solution after rigid body refinement. Red mesh indicates negative density at 3 sigma contour level; green mesh indicates positive density at 3 sigma contour level. Initial model is shown superposed with density. The largest red mesh peaks correspond to the cytosolic end of M1D2 helix and part of the M1D3 helix indicating the model needs adjustments in these regions.

(TIF)

**S10 Fig. Control experiments for cysteine residues introduced in D1-D2 domain.** a) Q115C, b) V126C, and d) V130C. Size exclusion chromatography profiles (left) and <sup>86</sup>Rb<sup>+</sup> uptake (center) values at 0 and 60 min of KtrAB complexes formed by KtrA<sub>C0</sub> and KtrB mutants with ATP and ADP. For V126C, the time course of modification by DTNB is also shown (right); for the other mutants, the equivalent data is presented in the main text. Closed arrowhead indicates elution volume of KtrAB complex; open arrowhead indicates elution volume of individual components. All mutants form a complex with KtrA<sub>C0</sub> in the presence of ATP or ADP, and retain the functional stimulation by ATP relative to ADP. SDS-PAGE of size-exclusion fractions are shown as insets. Inset in a) 1- KtrA+KtrB<sub>Q115C</sub> with ADP eluting at closed arrow; 2- KtrA+KtrB<sub>Q115C</sub> with ADP eluting at open arrow; 3- KtrA+KtrB<sub>Q115C</sub> with ATP eluting at closed arrow; 4- KtrA+KtrB<sub>Q115C</sub> with ATP eluting at open arrow; Inset in b) 1- KtrA+KtrB<sub>V126C</sub> with ADP eluting at closed arrow; 2- KtrA+KtrB<sub>V126C</sub> with ADP eluting at open arrow; 3- sample buffer; 4- KtrA+KtrB<sub>V126C</sub> with ATP eluting at closed arrow; 5- KtrA+KtrB<sub>V126C</sub> with ATP eluting at open arrow. Inset in c) 1- pure KtrB<sub>V130C</sub>; 2- KtrA+KtrB<sub>V130C</sub>



with ADP eluting at closed arrow; 3- KtrA+KtrB<sub>V130C</sub> with ADP eluting at open arrow; 4- KtrA+KtrB<sub>V130C</sub> with ATP eluting at closed arrow; 5- KtrA+KtrB<sub>V130C</sub> with ATP eluting at open arrow. Lower horizontal arrow indicates KtrA; horizontal arrow with M indicates KtrB monomer. Numerical values are included in [S1 Data](#). (TIF)

**S11 Fig. Control experiments for cytosolic pore cysteines.** **a)** N119C, **b)** P121C, **d)** F443C and **e)** T444C. Size exclusion chromatography profiles (left) and <sup>86</sup>Rb<sup>+</sup> uptake (right) values at 0 and 60 min of KtrAB complexes formed by KtrA<sub>C0</sub> and KtrB mutants with ATP and ADP. Closed arrowhead indicates elution volume of KtrAB complex; open arrowhead indicates elution volume of individual components. All mutants form a complex with KtrA<sub>C0</sub> in the presence of ATP or ADP and retain the functional stimulation by ATP relative to ADP, although reduced in F443C. SDS-PAGE of size-exclusion fractions are shown as insets. Inset in **a)** 1- KtrA+KtrB<sub>N119C</sub> with ADP eluting at closed arrow; 2- KtrA+KtrB<sub>N119C</sub> with ADP eluting at open arrow; 3- KtrA+KtrB<sub>N119C</sub> with ATP eluting at closed arrow; 4- KtrA+KtrB<sub>N119C</sub> with ATP eluting at open arrow; Inset in **b)** 1- pure KtrB<sub>P121C</sub>. 2- KtrA+KtrB<sub>P121C</sub> with ADP eluting at closed arrow; 3- KtrA+KtrB<sub>P121C</sub> with ADP eluting at open arrow; 4- KtrA+KtrB<sub>P121C</sub> with ATP eluting at closed arrow; 5- KtrA+KtrB<sub>P121C</sub> with ATP eluting at open arrow. Inset in **c)** 1- pure KtrB<sub>F443C</sub>. 2- KtrA+KtrB<sub>F443C</sub> with ADP eluting at closed arrow; 3- KtrA+KtrB<sub>F443C</sub> with ADP eluting at open arrow; 4- KtrA+KtrB<sub>F443C</sub> with ATP eluting at closed arrow; 5- KtrA+KtrB<sub>F443C</sub> with ATP eluting at open arrow. Inset in **d)** 1- pure KtrA; 2- pure KtrA; 3- pure KtrB<sub>T444C</sub>; 4- KtrA+KtrB<sub>T444C</sub> with ADP eluting at closed arrow; 5- KtrA+KtrB<sub>T444C</sub> with ATP eluting at closed arrow. Lower horizontal arrow indicates KtrA; horizontal arrow with M indicates KtrB monomer. Numerical values are included in [S1 Data](#). (TIF)

**S12 Fig. SDS-PAGE of size-exclusion fractions of KtrB<sub>Δloop</sub>, KtrB<sub>G306S</sub>, and KtrB<sub>S309D</sub>.** **a)** KtrB<sub>Δloop</sub>. Lanes 1 to 3 correspond to 1 ml fractions from chromatography of KtrA+KtrB<sub>Δloop</sub> with ADP ([Fig 5A](#)) collected around open arrow peak. Lanes 4 to 8 correspond to 1 ml fractions from chromatography of KtrA+KtrB<sub>Δloop</sub> with ATP ([Fig 5A](#)), starting at closed arrow and covering the open arrow peak. **b)** KtrB<sub>G306S</sub>. 1- pure KtrA; 2- KtrB<sub>G306S</sub> before size-exclusion; 3- KtrA+ KtrB<sub>G306S</sub> with ADP at open arrow; 4- KtrA+ KtrB<sub>G306S</sub> with ATP at open arrow. **c)** KtrB<sub>S309D</sub>. 1- pure KtrA; 2- KtrB<sub>S309D</sub> before size-exclusion; 3- KtrA+ KtrB<sub>S309D</sub> with ADP at open arrow; 4- KtrA+ KtrB<sub>S309D</sub> with ATP at open arrow. Lower horizontal arrow indicates KtrA; horizontal arrow with M indicates KtrB monomer. (TIF)

**S13 Fig. Western blots of fractions collected from float-up experiments.** Westerns were probed with anti-KtrB antibody. Fractions 1 to 5 correspond to 40 μl fractions collected from low to high sucrose concentration with liposomes floating to the low density fractions. KtrB float-up distribution for **a)** wild type KtrB and KtrB<sub>Δloop</sub> reconstituted liposomes; **b)** wild type KtrB and KtrB<sub>R417K</sub> reconstituted liposomes or **c)** KtrAB<sub>R417K</sub>-ATP and -ADP reconstituted liposomes. The membrane protein is detected in the low sucrose concentration fractions, showing that it is associated with the liposomes. Horizontal arrows with M or D indicate KtrB monomer or dimer, respectively. (TIF)

**S1 Table. Averaged absolute <sup>86</sup>Rb<sup>+</sup> uptake levels (counts per minute) of functional assays depicted in Fig 1.** Tables show the averaged raw data (before valinomycin normalization) collected for the KtrA<sub>ΔC</sub>B and KtrAB functional assays plotted in [Fig 1A and 1B](#), respectively. The increased background values seen in the KtrA<sub>ΔC</sub>B functional assay are explained by the much

lower valinomycin values for the Control time course in KtrA<sub>ΔC</sub>B (~26,000 cpm) relative to the same values in KtrAB (~54,000 cpm). The valinomycin values are obtained at the end of the time course and are used for normalization of the Rb<sup>+</sup> uptake, as a consequence normalized values for the KtrA<sub>ΔC</sub>B control are larger than for the KtrAB control. It is important to realize that in all biochemical and functional assays, we use an excess of RCK ring to favor the formation of the KtrAB complex, which has 1 dimer and 1 ring and minimize the formation of the complex with 1 RCK ring and 2 dimers of KtrB (see [S4 Fig](#)). In these circumstances, control liposomes were formed in the presence of KtrA<sub>ΔC</sub> and contain a large amount of free ring; in contrast, in liposomes reconstituted with KtrA<sub>ΔC</sub>B, a large fraction of the ring is involved in the formation of the complex. We do not know why KtrA<sub>ΔC</sub> appears to increase leakiness while full-length KtrA does not. The normalized data plotted in [Fig 1](#) are slightly different from normalized values calculated with data shown in [S1 Table](#). For [Fig 1](#), we first normalized each individual time course using the corresponding valinomycin value and then calculated the average for each timepoint. In [S1 Table](#), the values for a particular time point or valinomycin addition are the average of different sample preparations, reconstitutions, and time courses prior to normalization.

(DOCX)

**S2 Table. Diffraction data and refinement statistics.** Rmsd: root-mean-square deviation; values in parenthesis correspond to highest resolution bin.

(DOCX)

**S3 Table. Log of likelihood values for molecular replacement analysis.** \* - Incorrect packing between KtrB and the octameric ring. Molecular replacement functions for the wild-type KtrAB-ADP 8 Å diffraction dataset were calculated with PHASER and search models composed by KtrB homodimers from either the KtrAB-ATP or KtrA<sub>ΔC</sub>B-ADP structures and KtrA octameric rings adopting different conformations (after removing their C-terminal domains). The procedure involved sequential searches with the membrane protein and the gating ring; for many of these pairs, we were able to obtain molecular replacement solutions that display the expected packing between the membrane protein dimer and the gating ring. The values for the LLG function are a measure of how well the structural model agrees with the data. The pair formed by the KtrB homodimer and KtrA<sub>ΔC</sub> ring both from KtrA<sub>ΔC</sub>B-ADP has the highest LLG value (LLG = 515) and therefore appears to fit the data better than the other models. To evaluate the sensitivity of LLG parameter to small improvements in the KtrB model (in particular, the capacity of LLG to distinguish the goodness of fit between search models 6 and 7), we performed a series of tests. We first distorted the KtrB search model from KtrA<sub>ΔC</sub>B-ADP with a 10° tilt (see below explanation for this tilt) of the cytosolic halves of the M1D1 (residues 15 to 29) or M1D3 (residues 227–241) helices. This conformational change has not been observed in any of the existing structures, and so with this tilting the new KtrB search models are distorted (worsened) relative to KtrA<sub>ΔC</sub>B-ADP and KtrAB-ATP. Molecular replacement searches were performed with PHASER using the distorted KtrB dimers together with KtrA<sub>ΔC</sub> against the KtrAB-ADP 8 Å data. If the LLG parameter calculated in the search is sensitive to a distortion affecting 15 residues, then its values should be lower than 515, the value found for the final refined model of KtrA<sub>ΔC</sub>B-ADP; LLG for the model distorted at M1D1 was 506, and at M1D3 it was 503. For both cases, the packing of the different components was correct. This demonstrates that LLG is sensitive even to relatively small distortions of the search model. It also shows that even small changes in LLG (in these cases changes of less than 10%) indicate a model that is a worse or better fit to the data. We then altered KtrB of KtrAB-ATP. We changed the cytosolic half (residues 128 to 140) of the M1D2 helix in so that it coincides with the helices of the KtrB search model in KtrA<sub>ΔC</sub>B-ADP. We called this new model KtrB<sub>improved</sub>.

We performed the inverse operation on the KtrB search model of KtrA<sub>ΔC</sub>B-ADP so that it resembles KtrAB-ATP and called it KtrB<sub>worse</sub>. These changes corresponded to a 10–11° tilt of the cytosolic ends of the M1D2 helices around a pivot point, residue 140. Once again, if LLG is sensitive to these changes, then molecular replacement searches using KtrB<sub>improved</sub> (together with KtrA<sub>ΔC</sub>) against the KtrAB-ADP 8 Å data should show an increase in LLG relative to the unmodified model, while KtrB<sub>worse</sub> should result in a decrease in LLG relative to the unmodified model. KtrB<sub>improved</sub> LLG went up from 473 to 496 while for KtrB<sub>worse</sub> LLG went down from 515 to 496. Note also that the LLG value for KtrB<sub>improved</sub> is still lower than 515, the value obtained with the components of KtrA<sub>ΔC</sub>B; this shows that besides the difference in the M1D2 helices, there are many other small adjustments that occurred during refinement of KtrA<sub>ΔC</sub>B-ADP. These small adjustments improved the model and made it even more like KtrAB-ADP so that the LLG value is the highest. Overall, these experiments demonstrate how sensitive LLG in Phaser is to the goodness of fit of a search model to a crystal structure. Moreover, they demonstrate that the difference between 473 and 515 shown in the two bottom searches listed on [S3 Table](#) is significant, supporting our conclusion that the conformation of both the membrane protein and the RCK ring in full-length KtrAB-ADP is similar to the conformations observed in our KtrA<sub>ΔC</sub>B-ADP structure.

(DOCX)

## Acknowledgments

We are grateful for access to Proxima2 and Proxima1 at SOLEIL and to ID14-4/ID-29 at ESRF (through the Portuguese BAG), and thank the respective support staff. We thank Carol Harley for critical reading of the manuscript.

## Author Contributions

Conceived and designed the experiments: AS JHMC. Performed the experiments: AS RSVP CMTD RR JHMC. Analyzed the data: AS RSVP CMTD RR JHMC. Wrote the paper: AS JHMC.

## References

- Durell SR, Hao Y, Nakamura T, Bakker EP, Guy HR. Evolutionary relationship between K(+) channels and symporters. *Biophys J*. 1999 Aug; 77(2):775–88. PMID: [10423425](#)
- Corratge-Faillie C, Jabnoute M, Zimmermann S, Very AA, Fizames C, Sentenac H. Potassium and sodium transport in non-animal cells: the Trk/Ktr/HKT transporter family. *Cell Mol Life Sci*. 2010 Aug; 67(15):2511–32. doi: [10.1007/s00018-010-0317-7](#) PMID: [20333436](#)
- Rhoads DB, Waters FB, Epstein W. Cation transport in *Escherichia coli*. VIII. Potassium transport mutants. *J Gen Physiol*. 1976 Mar; 67(3):325–41. PMID: [4578](#)
- Diskowski M, Mikusevic V, Stock C, Hanelt I. Functional diversity of the superfamily of K+ transporters to meet various requirements. *Biol Chem*. 2015 Apr 2.
- Vieira-Pires RS, Szollosi A, Morais-Cabral JH. The structure of the KtrAB potassium transporter. *Nature*. 2013 Apr 18; 496(7445):323–8. doi: [10.1038/nature12055](#) PMID: [23598340](#)
- Holtmann G, Bakker EP, Uozumi N, Bremer E. KtrAB and KtrCD: two K+ uptake systems in *Bacillus subtilis* and their role in adaptation to hypertonicity. *J Bacteriol*. 2003 Feb; 185(4):1289–98. PMID: [12562800](#)
- Durell SR, Guy HR. Structural models of the KtrB, TrkH, and Trk1,2 symporters based on the structure of the KcsA K(+) channel. *Biophys J*. 1999 Aug; 77(2):789–807. PMID: [10423426](#)
- Kroning N, Willenborg M, Tholema N, Hanelt I, Schmid R, Bakker EP. ATP binding to the KTN/RCK subunit KtrA from the K+ -uptake system KtrAB of *Vibrio alginolyticus*: its role in the formation of the KtrAB complex and its requirement in vivo. *J Biol Chem*. 2007 May 11; 282(19):14018–27. PMID: [17344221](#)

9. Jiang Y, Pico A, Cadene M, Chait BT, MacKinnon R. Structure of the RCK domain from the E. coli K<sup>+</sup> channel and demonstration of its presence in the human BK channel. *Neuron*. 2001 Mar; 29(3):593–601. PMID: [11301020](#)
10. Roosild TP, Miller S, Booth IR, Choe S. A mechanism of regulating transmembrane potassium flux through a ligand-mediated conformational switch. *Cell*. 2002 Jun 14; 109(6):781–91. PMID: [12086676](#)
11. Albright RA, Ibar JL, Kim CU, Gruner SM, Morais-Cabral JH. The RCK domain of the KtrAB K<sup>+</sup> transporter: multiple conformations of an octameric ring. *Cell*. 2006 Sep 22; 126(6):1147–59. PMID: [16990138](#)
12. Jiang Y, Lee A, Chen J, Cadene M, Chait BT, MacKinnon R. The open pore conformation of potassium channels. *Nature*. 2002 May 30; 417(6888):523–6. PMID: [12037560](#)
13. Jiang Y, Lee A, Chen J, Cadene M, Chait BT, MacKinnon R. Crystal structure and mechanism of a calcium-gated potassium channel. *Nature*. 2002 May 30; 417(6888):515–22. PMID: [12037559](#)
14. Yuan P, Leonetti MD, Pico AR, Hsiung Y, MacKinnon R. Structure of the human BK channel Ca<sup>2+</sup>-activation apparatus at 3.0 Å resolution. *Science*. 2010 Jul 9; 329(5988):182–6. doi: [10.1126/science.1190414](#) PMID: [20508092](#)
15. Yuan P, Leonetti MD, Hsiung Y, MacKinnon R. Open structure of the Ca<sup>2+</sup> gating ring in the high-conductance Ca<sup>2+</sup>-activated K<sup>+</sup> channel. *Nature*. 2012 Jan 5; 481(7379):94–7.
16. Wu Y, Yang Y, Ye S, Jiang Y. Structure of the gating ring from the human large-conductance Ca<sup>2+</sup>-gated K<sup>+</sup> channel. *Nature*. 2010 Jul 15; 466(7304):393–7. doi: [10.1038/nature09252](#) PMID: [20574420](#)
17. Kong C, Zeng W, Ye S, Chen L, Sauer DB, Lam Y, et al. Distinct gating mechanisms revealed by the structures of a multi-ligand gated K<sup>+</sup> channel. *Elife*. 2012; 1:e00184. doi: [10.7554/eLife.00184](#) PMID: [23240087](#)
18. Cao Y, Pan Y, Huang H, Jin X, Levin EJ, Kloss B, et al. Gating of the TrkH ion channel by its associated RCK protein TrkA. *Nature*. 2013 Apr 18; 496(7445):317–22. doi: [10.1038/nature12056](#) PMID: [23598339](#)
19. Durell SR, Bakker EP, Guy HR. Does the KdpA subunit from the high affinity K<sup>+</sup>-translocating P-type KDP-ATPase have a structure similar to that of K<sup>+</sup> channels? *Biophys J*. 2000 Jan; 78(1):188–99. PMID: [10620285](#)
20. Cao Y, Jin X, Huang H, Derebe MG, Levin EJ, Kabaleswaran V, et al. Crystal structure of a potassium ion transporter, TrkH. *Nature*. 2011 Mar 17; 471(7338):336–40. doi: [10.1038/nature09731](#) PMID: [21317882](#)
21. Hanelt I, Lochte S, Sundermann L, Elbers K, Vor der Bruggen M, Bakker EP. Gain of function mutations in membrane region M2C2 of KtrB open a gate controlling K<sup>+</sup> transport by the KtrAB system from *Vibrio alginolyticus*. *J Biol Chem*. 2010 Apr 2; 285(14):10318–27. doi: [10.1074/jbc.M109.089870](#) PMID: [20097755](#)
22. Hanelt I, Wunnicke D, Muller-Trimbusch M, Vor der Bruggen M, Kraus I, Bakker EP, et al. Membrane region M2C2 in subunit KtrB of the K<sup>+</sup> uptake system KtrAB from *Vibrio alginolyticus* forms a flexible gate controlling K<sup>+</sup> flux: an electron paramagnetic resonance study. *J Biol Chem*. 2010 Sep 3; 285(36):28210–9. doi: [10.1074/jbc.M110.139311](#) PMID: [20573964](#)
23. Bai Y, Yang J, Zarrella TM, Zhang Y, Metzger DW, Bai G. Cyclic di-AMP impairs potassium uptake mediated by a cyclic di-AMP binding protein in *Streptococcus pneumoniae*. *J Bacteriol*. 2014 Feb; 196(3):614–23. doi: [10.1128/JB.01041-13](#) PMID: [24272783](#)
24. Kim H, Youn SJ, Kim SO, Ko J, Lee JO, Choi BS. Structural Studies of Potassium Transport Protein KtrA Regulator of Conductance of K<sup>+</sup> (RCK) C Domain in Complex with Cyclic Diadenosine Monophosphate (c-di-AMP). *J Biol Chem*. 2015 Jun 26; 290(26):16393–402. doi: [10.1074/jbc.M115.641340](#) PMID: [25957408](#)
25. Corrigan RM, Campeotto I, Jeganathan T, Roelofs KG, Lee VT, Grundling A. Systematic identification of conserved bacterial c-di-AMP receptor proteins. *Proc Natl Acad Sci U S A*. 2013 May 28; 110(22):9084–9. doi: [10.1073/pnas.1300595110](#) PMID: [23671116](#)
26. Nelson JW, Sudarsan N, Furukawa K, Weinberg Z, Wang JX, Breaker RR. Riboswitches in eubacteria sense the second messenger c-di-AMP. *Nat Chem Biol*. 2013 Dec; 9(12):834–9. doi: [10.1038/nchembio.1363](#) PMID: [24141192](#)
27. Ellman GL. Tissue sulfhydryl groups. *Arch Biochem Biophys*. 1959 May; 82(1):70–7. PMID: [13650640](#)
28. Czernski L, Sanders CR. Thiol modification of diacylglycerol kinase: dependence upon site membrane disposition and reagent hydrophobicity. *FEBS Lett*. 2000 Apr 28; 472(2–3):225–9. PMID: [10788616](#)
29. Vopel T, Kunzelmann S, Herrmann C. Nucleotide dependent cysteine reactivity of hGBP1 uncovers a domain movement during GTP hydrolysis. *FEBS Lett*. 2009 Jun 18; 583(12):1923–7. doi: [10.1016/j.febslet.2009.05.027](#) PMID: [19463820](#)

30. Kato N, Akai M, Zulkifli L, Matsuda N, Kato Y, Goshima S, et al. Role of positively charged amino acids in the M2D transmembrane helix of Ktr/Trk/HKT type cation transporters. *Channels (Austin)*. 2007 May-Jun; 1(3):161–71.
31. Zhang J, Xue F, Liu Y, Yang H, Wang X. The structural mechanism of the Cys-loop receptor desensitization. *Mol Neurobiol*. 2013 Aug; 48(1):97–108. doi: [10.1007/s12035-013-8420-z](https://doi.org/10.1007/s12035-013-8420-z) PMID: [23397136](https://pubmed.ncbi.nlm.nih.gov/23397136/)
32. Lester HA, Dibas MI, Dahan DS, Leite JF, Dougherty DA. Cys-loop receptors: new twists and turns. *Trends Neurosci*. 2004 Jun; 27(6):329–36. PMID: [15165737](https://pubmed.ncbi.nlm.nih.gov/15165737/)
33. Meyerson JR, Kumar J, Chittori S, Rao P, Pierson J, Bartesaghi A, et al. Structural mechanism of glutamate receptor activation and desensitization. *Nature*. 2014 Oct 16; 514(7522):328–34. doi: [10.1038/nature13603](https://doi.org/10.1038/nature13603) PMID: [25119039](https://pubmed.ncbi.nlm.nih.gov/25119039/)
34. Chaudhry C, Weston MC, Schuck P, Rosenmund C, Mayer ML. Stability of ligand-binding domain dimer assembly controls kainate receptor desensitization. *EMBO J*. 2009 May 20; 28(10):1518–30. doi: [10.1038/emboj.2009.86](https://doi.org/10.1038/emboj.2009.86) PMID: [19339989](https://pubmed.ncbi.nlm.nih.gov/19339989/)
35. Ye S, Li Y, Chen L, Jiang Y. Crystal structures of a ligand-free MthK gating ring: insights into the ligand gating mechanism of K<sup>+</sup> channels. *Cell*. 2006 Sep 22; 126(6):1161–73. PMID: [16990139](https://pubmed.ncbi.nlm.nih.gov/16990139/)
36. Li W, Aldrich RW. State-dependent block of BK channels by synthesized shaker ball peptides. *J Gen Physiol*. 2006 Oct; 128(4):423–41. PMID: [16966472](https://pubmed.ncbi.nlm.nih.gov/16966472/)
37. Liu Y, Holmgren M, Jurman ME, Yellen G. Gated access to the pore of a voltage-dependent K<sup>+</sup> channel. *Neuron*. 1997 Jul; 19(1):175–84. PMID: [9247273](https://pubmed.ncbi.nlm.nih.gov/9247273/)
38. Holmgren M, Smith PL, Yellen G. Trapping of organic blockers by closing of voltage-dependent K<sup>+</sup> channels: evidence for a trap door mechanism of activation gating. *J Gen Physiol*. 1997 May; 109(5):527–35. PMID: [9154902](https://pubmed.ncbi.nlm.nih.gov/9154902/)
39. Rothberg BS, Shin KS, Phale PS, Yellen G. Voltage-controlled gating at the intracellular entrance to a hyperpolarization-activated cation channel. *J Gen Physiol*. 2002 Jan; 119(1):83–91. PMID: [11773240](https://pubmed.ncbi.nlm.nih.gov/11773240/)
40. Uysal S, Cuello LG, Cortes DM, Koide S, Kossiakoff AA, Perozo E. Mechanism of activation gating in the full-length KcsA K<sup>+</sup> channel. *Proc Natl Acad Sci U S A*. 2011 Jul 19; 108(29):11896–9. doi: [10.1073/pnas.1105112108](https://doi.org/10.1073/pnas.1105112108) PMID: [21730186](https://pubmed.ncbi.nlm.nih.gov/21730186/)
41. Kabsch W. Xds. *Acta Crystallogr D Biol Crystallogr*. 2010 Feb; 66(Pt 2):125–32. doi: [10.1107/S0907444909047337](https://doi.org/10.1107/S0907444909047337) PMID: [20124692](https://pubmed.ncbi.nlm.nih.gov/20124692/)
42. Winn MD, Ballard CC, Cowtan KD, Dodson EJ, Emsley P, Evans PR, et al. Overview of the CCP4 suite and current developments. *Acta Crystallogr D Biol Crystallogr*. 2011 Apr; 67(Pt 4):235–42. doi: [10.1107/S0907444910045749](https://doi.org/10.1107/S0907444910045749) PMID: [21460441](https://pubmed.ncbi.nlm.nih.gov/21460441/)
43. Adams PD, Afonine PV, Bunkoczi G, Chen VB, Davis IW, Echols N, et al. PHENIX: a comprehensive Python-based system for macromolecular structure solution. *Acta Crystallogr D Biol Crystallogr*. 2010 Feb; 66(Pt 2):213–21. doi: [10.1107/S0907444909052925](https://doi.org/10.1107/S0907444909052925) PMID: [20124702](https://pubmed.ncbi.nlm.nih.gov/20124702/)
44. Brunger AT, Adams PD, Fromme P, Fromme R, Levitt M, Schroder GF. Improving the accuracy of macromolecular structure refinement at 7 Å resolution. *Structure*. 2012 Jun 6; 20(6):957–66. doi: [10.1016/j.str.2012.04.020](https://doi.org/10.1016/j.str.2012.04.020) PMID: [22681901](https://pubmed.ncbi.nlm.nih.gov/22681901/)